Journal of Civil Engineering and Urbanism

Volume 3, Issue 5: 265-278 (2013) (Received: June 20, 2013; Accepted: August 21, 2013; Published: September 30, 2013) **ISSN-2252-0430**

Errors Estimation of Different Numerical Integration Techniques on Stiffness Matrix and Stress Intensity Factor in XFEM

Hamed Ghohani Arab[1], Mohammad Reza Ghasemi [2]*

[1]*Ph.D. Student, Civil Engineering Department, University of Sistan and Baluchestan, Zahedan, 9816745639, Iran*
[2]*Associate Professor, Civil Engineering Department, University of Sistan and Baluchestan, Zahedan, 9816745639, Iran*

*Corresponding author's Email address: mrghasemi@hamoon.usb.ac.ir

ABSTRACT: One of the new methods in the analysis of cracked structures is extended Finite Element Method (XFEM). In this method, unlike the conventional finite element method to calculate the integral of stiffness matrix using Gauss quadrature rule, accuracy of stiffness matrix of cracked elements is reduced. This article builds on the relationship between errors in the calculations if one uses different methods to calculate the stiffness matrix integral. The three methods of integration used and presented here are trapezoidal rule integration, Gauss quadrature integration and sub element rule integration. The average stiffness matrix error and maximum stiffness matrix errors were considered as the assessing criteria. L2-norm and energy norm criteria were also used. Finally accuracy of stress intensity factor (SIF) determined by XFEM were compared with different integration rules conventionally used in the literature.

Keywords: Gauss Quadrature Integration, SIF ,Stiffness Matrix, Sub Element Rule Integration, Trapezoidal Rule Integration, XFEM

ORIGINAL ARTICLE

INTRODUCTION

Normally engineering problems could be encountered with dilemma such as discontinuities, singularities, high gradients or other non-smooth properties. In solid mechanics, such problems may be due to cracks, shear bands, dislocations, inclusions and voids (Fries and Belytschko, 2010).

In the present study, emphasize has been addressed to cracks. In dealing with this type of problem, two methods have been introduced in the literature. One strategy is to use polynomial approximation, where a mesh concur the discontinuities, followed by refining the mesh in the vicinity of regions with singularities and high stress gradients. This may be regarded as a drawback of Finite Element Method where remeshing is required (Belytschko et al., 2000; Zienkiewicz and Taylor, 2000).

In the second strategy the singular or discontinuous displacement field within a finite element is simulated by a special set of enriched shape functions that allow for accurate approximation of the displacement field (Moës et al., 1999). The main advantage of this method is that it does not require any remeshing in the process of crack propagation. By advancement of the crack tip location or any change in its path due to loading conditions, the method automatically determines the elements around the crack path/tip and generates necessary enrichment functions for the associated finite elements or nodal points accordingly (Mohammadi, 2008).

We focus on mesh based enrichment methods which realize the enrichment extrinsically by the partition of unity concept. The basic ideas and the mathematical foundation of the Partition of Unity Finite Element Method (PUFEM) were discussed by Melenk and Babuska (1996) and Duarte and Oden (1996). Later Belytschko and Black (1999) presented a minimal remeshing finite element method by adding discontinuous enrichment functions to the finite element approximation to account for the presence of a crack. The method was then improved by Moës et al. (1999) and Dolbow (1999) where it was called the eXtended Finite Element Method (XFEM). This methodology allowed for the entire crack to be represented independently of the mesh and constructed the enriched approximation from the interaction of the crack geometry with the mesh. More contributions from Dolbow et al. (2000a,b, 2001), Daux et al. (2000) and Sukumar et al. (2000) extended the method for three-dimensional crack modeling and arbitrary branched and intersecting cracks.

MATERIALS AND METHODS

Extended Finite Element Method (XFEM)

In contrast to the classical finite element method where crack surfaces are explicitly meshed and must conform to mesh boundaries, in XFEM, inter-element crack discontinuities are modeled entirely independent of the underlying mesh. Thus, cracks are represented via the displacement approximation enriching the classical displacement based approximation by a function that is discontinuous across the crack permits crack modeling to be realized. The enriched displacement field in the X-

FEM is given by (Motamedi and Mohammadi, 2010; Pommier et al., 2011):

$$u^h(x)=\sum_{i\in I} d_i N_i(x)+\sum_{j\in L} b_j N_j(x) H(x) + \sum_{k_1\in K_1} N_{k_1}(x)\left(\sum_{l=1}^{4} c_{k_1,1}^{l} F_1^{l}(x)\right) + \sum_{k_2\in K_2} N_{k_2}(x)\left(\sum_{l=1}^{4} c_{k_2,2}^{l} F_2^{l}(x)\right) \quad (1)$$

where $N_i(x)$ is the polynomial basis function of node i, d_i are the classical degrees of freedom associated with node i. Coefficients b_j are the enriched degrees of freedom associated with node j and the Heaviside function $H(x)$ denotes discontinuity across the crack interior. The function $H(x)$ is +1 to the left of the crack and -1 to its right. $c^l_{i,1}$ and $c^l_{i,2}$ are the enriched degrees of freedom associated with nodes k_1 and k_2. I is the set of all nodes in the mesh, the set $K_1$and K_2 are the sets of nodes to be enriched in order to model the crack tips 1 and 2, respectively and J is the set of nodes whose basis function supports are cut by the crack interior and do not belong to set K. Figure 1 illustrates the Node selection for enrichment; the nodes marked by squares are enriched by crack-tip functions and the circled ones are enriched by the Heaviside function (Dolbow and Nadeau, 2002).

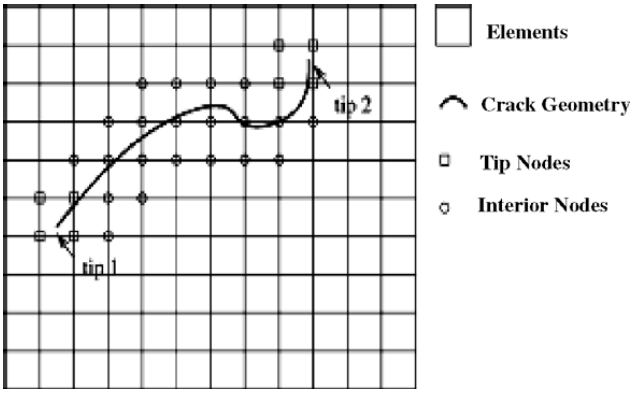

Figure 1. Node selection for enrichment (Dolbow and Nadeau, 2002)

The near-tip enrichment functions $F_1^l(x)$ and $F_2^l(x)$ are defined as (Bayesteh and Mohammadi, 2013):

$$\left\{F_{\alpha}^{l}(x), l=1,2,3,4\right\} \equiv \left\{\sqrt{r}\sin\sin\left(\frac{\theta}{2}\right), \sqrt{r}\cos\cos\left(\frac{\theta}{2}\right), \sqrt{r}\sin\sin\left(\frac{\theta}{2}\right)\sin\sin(\theta), \sqrt{r}\cos\cos\left(\frac{\theta}{2}\right)\sin\sin(\theta)\right\} \quad (2)$$

where r and θ as shown in Figure 2, are local crack-tip polar coordinates of point x.

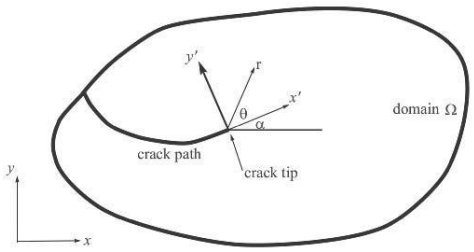

Figure 2. Polar coordinates at the crack tip (Mohammadi, 2008)

The discrete system of linear equations in the XFEM in global form can be written as (Sukumar and Prévost, 2003):

$$\mathbf{K}\mathbf{u}^h=\mathbf{f} \quad (3)$$

where **K** is the stiffness matrix, $\mathbf{u}^h$ is the vector of nodal degrees of freedom for both classical and enriched ones, and **f** is the vector of external force. The global matrix and vectors are calculated by assembling matrices and vectors of each element. **K** and **f** for each element are defined as (Asadpoure et al., 2006):

$$\mathbf{K}_{ij}^{e}=\int_{\Omega^e}\mathbf{B}_i^T\mathbf{D}\mathbf{B}_j d\Omega \quad (4)$$

$$\mathbf{f}_i^e=\left[\mathbf{f}_i^d \quad \mathbf{f}_i^a \quad \mathbf{f}_i^{b1} \quad \mathbf{f}_i^{b2} \quad \mathbf{f}_i^{b3} \quad \mathbf{f}_i^{b4}\right] \quad (5.1)$$

$$\mathbf{f}_i^d=\int_{\partial\Omega_t^h\cap\partial\Omega^e} N_i\bar{\mathbf{t}}d\Gamma+\int_{\Omega^e} N_i\mathbf{b}d\Omega \quad (5.2)$$

$$\mathbf{f}_i^a=\int_{\partial\Omega_t^h\cap\partial\Omega^e} N_i H\bar{\mathbf{t}}d\Gamma+\int_{\Omega^e} N_i H\mathbf{b}d\Omega \quad (5.3)$$

$$\mathbf{f}_i^{b\alpha}=\int_{\partial\Omega_t^h\bigcap\partial\Omega^e} N_i F_\alpha\bar{\mathbf{t}}d\Gamma+\int_{\Omega^e} N_i F_\alpha\mathbf{b}d\Omega \quad (5.4)$$

where Ω^e is an element, Ω_t^h is an element with a crack lying along its edges, $\partial\Omega$ denotes the boundary of the domain Ω, $\bar{t}$ is the traction and b is the body force. In Eq. (4), **B** is the matrix of shape function derivatives (Mohammadi, 2008):

$$\mathbf{B}_i=\left[\mathbf{B}_i^d \quad \mathbf{B}_i^a \quad \mathbf{B}_i^{b1} \quad \mathbf{B}_i^{b2} \quad \mathbf{B}_i^{b3} \quad \mathbf{B}_i^{b4}\right] \quad (6.1)$$

$$\mathbf{B}_i^d=\begin{bmatrix} N_{i,x} & 0 \\ 0 & N_{i,y} \\ N_{i,y} & N_{i,x}\end{bmatrix} \quad (6.2)$$

$$\mathbf{B}_i^a=\begin{bmatrix} (N_iH)_{,x} & 0 \\ 0 & (N_iH)_{,y} \\ (N_iH)_{,y} & (N_iH)_{,x}\end{bmatrix} \quad (6.3)$$

$$\mathbf{B}_i^{b\alpha}=\begin{bmatrix} (N_iF_\alpha)_{,x} & 0 \\ 0 & (N_iF_\alpha)_{,y} \\ (N_iF_\alpha)_{,y} & (N_iF_\alpha)_{,x}\end{bmatrix} \quad (6.4)$$

To cite this paper: H.Ghohani Arab, M.R. Ghasemi, 2013. Errors Estimation of Different Numerical Integration Techniques on Stiffness Matrix and Stress Intensity Factor in XFEM. *J. Civil Eng. Urban.*,3 (5): 265-278.
Journal homepage: http://www.ojceu.ir/main/

Numerical Integration

Consider the situation where the local enrichment functions have jumps or kinks within elements. Standard Gauss quadrature in the weak form as frequently used in the classical FEM requires smoothness of the integrands. In the presence of jumps or kinks the accuracy of Gauss quadrature and other methods that assume smoothness is drastically decreased. Therefore, for discontinuous enrichments, special procedures are required for the quadrature of the weak form (Fries and Belytschko, 2010).

Because the ordinary Gauss rules do not accurately calculate the integration of enrichment functions in elements cut by a crack, Dolbow (1999) proposed two methods to overcome this numerical difficulty. The first method is to subdivide the element at both sides of the crack into sub-triangles whose edges are adapted to crack faces. The second one is to subdivide the element into sub-quads. Both methods are illustrated in Figure 3.

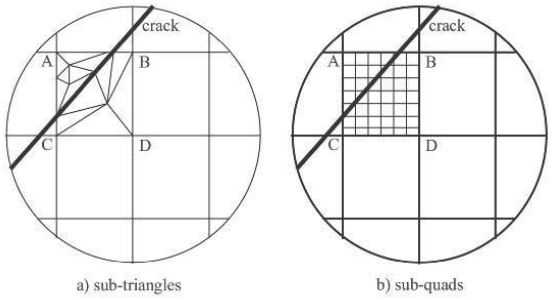

Figure 3. Methods 1 and 2 as (a) and (b) for partitioning the cracked element (Mohammadi, 2008)

In first method, for integration purposes, a decomposition of the elements into sub-elements that align with the discontinuity has been proposed in the early works on the XFEM, e.g. by Moës et al. (1999) and Sukumar et al. (2000). The sub-elements do not have to be conforming and no new unknowns are created from this decomposition (Fries and Belytschko, 2010).

In second method, those elements cut by the crack are divided into a grid of quadrilaterals, denoted as sub-quads, as shown in Figure 3. A trapezoidal rule can then be used in each sub-quad for integration purposes (Dolbow, 1999).

Due to high gradients near the singularity, a concentration of integration points in the vicinity of the singularity improves the results significantly. This can be achieved by using polar integration approaches as described in Laborde et al. (2005) and Béchet et al. (2005). Laborde et al. (2005) have shown that this approach eliminates the singular term from the quadrature. The idea is to decompose the element containing the crack tip into triangles, so that each triangle has one node at the singularity, known as singularity node. Tensor-product type Gauss points in a quadrilateral reference element are mapped into each triangle such that two nodes of the quadrilateral coincide at the singularity node of each triangle. The procedure is depicted in Figure 4. This approach is well suited for point singularities.

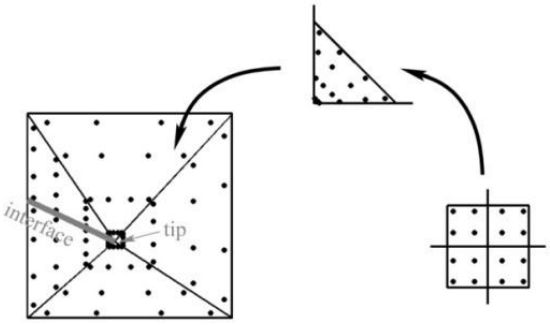

Figure 4. Integration points in an element containing a singularity (Fries and Belytschko, 2010)

Special integration points and weights are used which capture the singularity either at a node or along an edge of a sub-element resulting from a decomposition (Fries and Belytschko, 2010).

Standard Gauss points are projected from a quadrilateral element into a triangular element. The triangular element is then projected into the element containing the singularity such that the integration points are concentrated at the singularity (Fries and Belytschko, 2010).

Since the accuracy of the analysis depends on the precision of computed stiffness matrices for the members and the structure, in the present work therefore the effect of number of gauss points and the integration method were studied on the errors built. Thus the following criteria were considered to obtain the computed errors.

Errors Criteria

Stiffness matrix error: To compute the error in the stiffness matrix, we assumed that trapezoidal integration over the stiffness matrix may result a near exact solution when resembled with a 500×500 network of Gauss points. The two criteria for obtaining stiffness matrix error are defined as:

$$E_{\max} = \max\left(\frac{\left|K_{ij}^{500} - K_{ij}\right|}{K_{ij}^{500}}\right) \tag{7.1}$$

$$E_{ave} = \frac{1}{m}\sum_{i=1}^{n}\sum_{j=1}^{n}\left(\frac{\left|K_{ij}^{500} - K_{ij}\right|}{K_{ij}^{500}}\right) \tag{7.2}$$

where E_{max} and E_{ave} denote maximum and average error on the elements stiffness matrices. K_{ij}^{500} is the ijth element of stiffness matrix accounting for the trapezoidal integration with a 500×500 network. K_{ij} is the ijth element of stiffness matrix, n is the total degrees of freedom of the structure and m is the non-zero elements of stiffness matrix.

L_2-Norm Error Criterion: To compare the rate of produced element displacement error with the actual amount, L_2 formula is used where (Fries and Belytschko, 2007):

$$L_2 = \sqrt{\frac{\int\left(u_{ex} - u_{ap}\right)^2 dA}{\int u_{ex}^2 dA}} + \sqrt{\frac{\int\left(v_{ex} - v_{ap}\right)^2 dA}{\int v_{ex}^2 dA}} \tag{8}$$

Here, u_{ex} and v_{ex} denote actual horizontal and vertical displacements, while u_{ap} and v_{ap} are the corresponding computed values, respectively. u_{ex} and v_{ex} may be computed according to some arbitrary values for stress construction values, using Equation 9, stated as (Anderson, 1985):

$$\begin{Bmatrix} u_{ex} \\ v_{ex} \end{Bmatrix} = \frac{K_I}{2\mu}\sqrt{\frac{r}{2\pi}}\begin{Bmatrix} \cos(\theta/2)(\kappa-\cos(\theta)) \\ \sin(\theta/2)(\kappa-\cos(\theta)) \end{Bmatrix} + \frac{K_{II}}{2\mu}\sqrt{\frac{r}{2\pi}}\begin{Bmatrix} \sin(\theta/2)(2+\kappa+\cos(\theta)) \\ \cos(\theta/2)(2-\kappa-\cos(\theta)) \end{Bmatrix} \quad (9)$$

μ is being the shear modulus of elasticity. κ, as the Kolossov's constant, is obtained using either κ=(3-ν)/(1+ν) or κ=3-4ν formulae for the case of plane stress or plane strain, respectively. K_I and K_{II} are Stress Intensity Factors (SIFs) for modes I and II, respectively.

To determine v_{ap} and u_{ap}, via selecting an arbitrary stress concentration coefficient, and using Equation 9, nodal displacements for each element will be first found. XFEM will then be employed to do the analysis.

Integral computation of Equation 8 will be carried out using Gauss Quadrature, regarding a 20×20 network of sampling points.

Energy norm Criterion: Rate of absorbed energy error by each element *"E"* as in Equation 10, meaning to survey stress and strain error, is accomplished using energy norm criterion (Fries and Belytschko, 2007). Therefore:

$$E = \sqrt{\frac{\int \varepsilon_{ap}^T \sigma_{ap} dA}{\int \varepsilon_{ex}^T \sigma_{ex} dA}} \quad (10)$$

where σ_{ex} and ε_{ex} are the actual values for the stress and strain vectors. σ_{ap} and ε_{ap} are the computed values for the stress and strain vectors. The actual σ_{ex} values are determined through equation 11 and via using a selected coefficient for the stress intensity factor. Values for ε_{ex} are however found using the relation $\boldsymbol{\varepsilon}=\mathbf{D}^T.\boldsymbol{\sigma}$ (Anderson, 1985).

$$\begin{Bmatrix} \sigma_{xx} \\ \sigma_{yy} \\ \sigma_{xy} \end{Bmatrix} = \frac{K_I}{\sqrt{2\pi r}}\cos\left(\frac{\theta}{2}\right)\begin{Bmatrix} 1-\sin\left(\frac{\theta}{2}\right)\sin\left(\frac{3\theta}{2}\right) \\ 1+\sin\left(\frac{\theta}{2}\right)\sin\left(\frac{3\theta}{2}\right) \\ \sin\left(\frac{\theta}{2}\right)\cos\left(\frac{3\theta}{2}\right) \end{Bmatrix} + \frac{K_{II}}{\sqrt{2\pi r}}\begin{Bmatrix} -\sin\left(\frac{\theta}{2}\right)\left(2+\cos\left(\frac{\theta}{2}\right)\cos\left(\frac{3\theta}{2}\right)\right) \\ \sin\left(\frac{\theta}{2}\right)\cos\left(\frac{\theta}{2}\right)\cos\left(\frac{3\theta}{2}\right) \\ \cos\left(\frac{\theta}{2}\right)\left(1-\sin\left(\frac{\theta}{2}\right)\sin\left(\frac{3\theta}{2}\right)\right) \end{Bmatrix} \quad (11)$$

In order to determine values for σ_{ap} and ε_{ap} considering stress intensity factors is chosen and the amount of nodal elements displacements are calculated by equation 9 and then analysis is executed by means of XFEM method.

RESULTS AND DISCUSSION

To investigate on the accuracy of different integration techniques, eight different types of elements, as shown in Figure 5 will be inspected. Details of investigations carried out in each element type are described in the following sections.

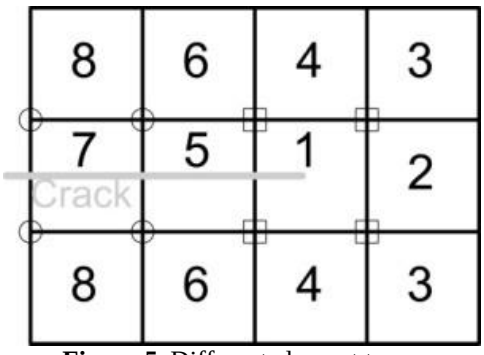

Figure 5. Different element types

Element type 1

Having placed the crack's tip inside this element, the crack tip enrichment was executed for all the corresponding nodes of the element. Integration was then carried out on the element, using three different integration rules as follows:

Trapezoidal rule integration: In this rule numbers of sampling points considered were within a 2*2 to 200*200 networks. It is worth to note that odd numbers of points were not considered since some of these points would lay on the discontinuity boundary and could simply cause problems during the procedure. The trend of average error of stiffness matrix with respect to the sub-quads, related to this rule, is shown in Figure 6.

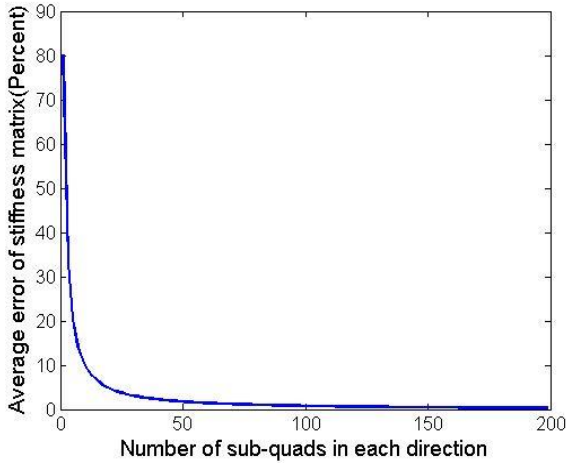

Figure 6 (a). Average error of stiffness matrix by Trapezoidal rule integration, related to Element's type 1

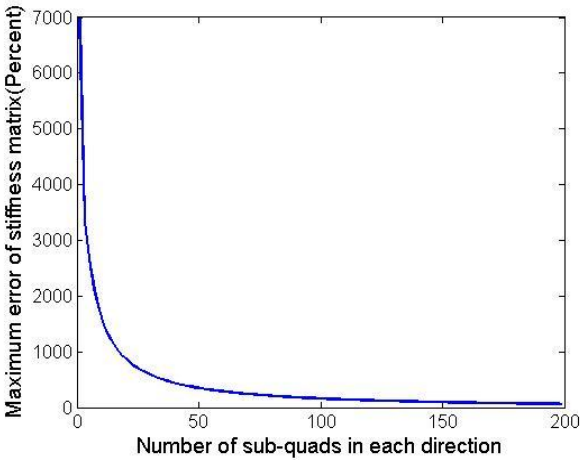

Figure 6 (b). Maximum error of stiffness matrix by Trapezoidal rule integration, related to Element's type 1

There, we observe that as sampling points increase error change gradient decreases. Considering a 81*81 network which means executing calculations for 6561 points, average error of stiffness matrix is found less than 1%. However maximum error of stiffness matrix never becomes less than 1%. Number of required sampling points to achieve a 2, 5 and 10 percent errors are listed in Table 1.

Gauss Quadrature integration: Here, the number of sampling points considered were within a range of 2*2 to 20*20 networks. The corresponding error history is shown in Figure 7.

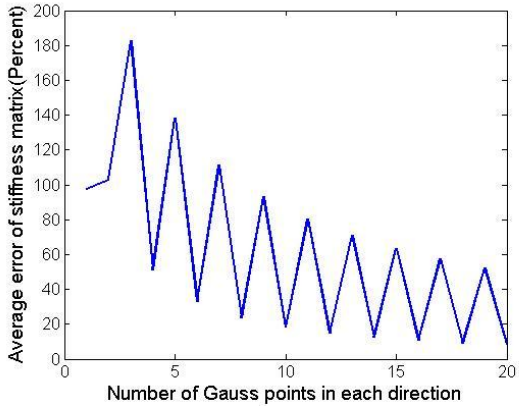

Figure 7(a). Average error of stiffness matrix by Gauss Quadrature integration, related to Element's type 1

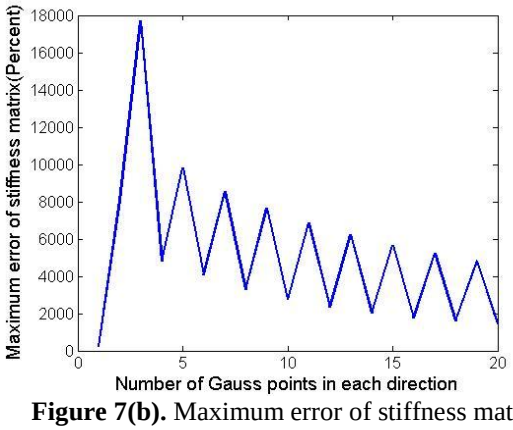

Figure 7(b). Maximum error of stiffness matrix by Gauss Quadrature integration, related to Element's type 1

Considering these diagrams we observe that as sampling points increase, error change gradient decreases. However the reduction rate is greater compared to trapezoidal rule integration. The disturbance created in these diagrams is due to the fact that when odd numbers sampling points are chosen a number of these points get placed on discontinuity boundary and when solving the calculations numerically they face problems. By considering a 20*20 network which means executing 400 calculations, the average error in stiffness matrix is equal to 8.25%. But maximum error in stiffness matrix is very high.

Sub elements rule integration: Here the element is divided into 6 sub elements as shown in Figure 8 and integration is executed in each sub element. Sampling points in each sub element were considered within a range of 2*2 to 20*20 networks. The convergence history of error corresponding to the stiffness matrix is shown in Figure 9.

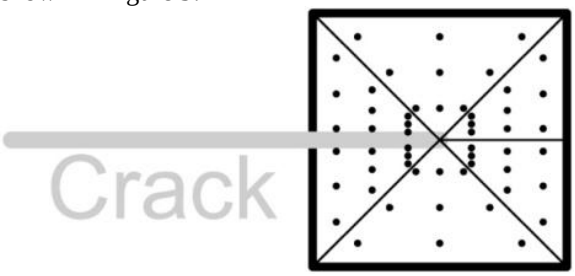

Figure 8. Sub elements of element type 1

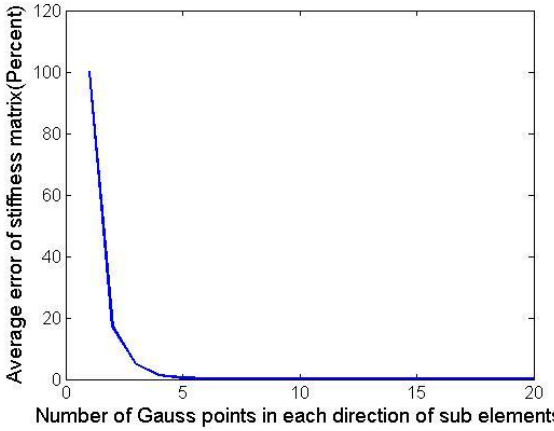

Figure 9(a). Average error of stiffness matrix by Sub elements rule integration, related to Element's type 1

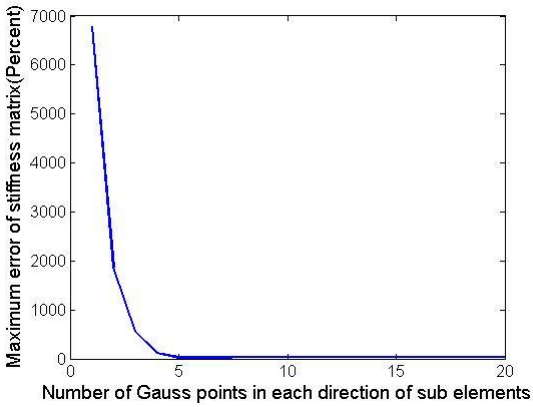

Figure 9(b). Maximum error of stiffness matrix by Sub elements rule integration Element's type 1

Considering these diagrams we observe that as the number of sampling points increases the error decreases. But the gradient decrease is more announced compared to trapezoidal and Gauss Quadrature rules integrations. Average error in stiffness matrix for a 5*5 network in each sub element, was found less than 1%.

Table 1. Required minimum number of sampling points leading to different errors for element type 1

Type of integration	Trape-zoidal rule	Gauss Quad-rature rule	Sub elemen-ts rule
Required number of sampling points to achieve a less than 2% average error	44*44	---	6*4*4
Required number of sampling points to achieve a less than 2% maximum error	---	---	---
Required number of sampling points to achieve a less than 5% average error	19*19	---	6*3*3
Required number of sampling points to achieve a less than 5% maximum error	---	---	---
Required number of sampling points to achieve a less than 10% average error	11*11	18*18	6*3*3
Required number of sampling points to achieve a less than 10% maximum error	---	---	---

Considering the high maximum error of stiffness matrix, L_2–norm and Energy norm Criteria were also considered for this element type. The problem was solved once by the assumption of K_{II}=0 & K_I= 1 and the other time by the assumption of K_{II}=1 & K_I= 0. The results obtained are displayed in Figure 10.

As is evident from Figure 10 it is clear that error reduction becomes almost fixed to a very small value while increasing number of sampling points from 3*3 networks in each sub element to 20*20. Therefore we notice that if we use the sub element integration considering a 5*5 network in each sub element by executing minimum calculations we can reach an acceptable accuracy in calculations related to stiffness matrix.

Note that in determining all error discrepancies, different element sizes were studied and it was observed that elements size is not effective in the magnitude of the error.

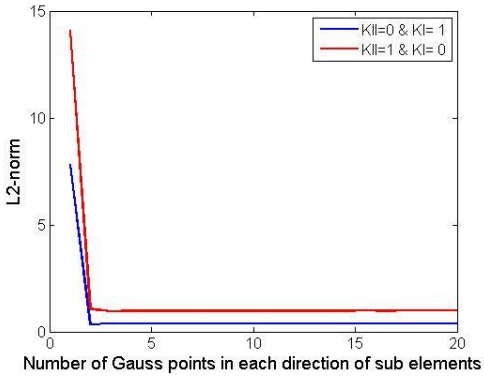

Figure 10(a). Convergence history of L_2 norm with number of Gauss points for element type 1 by Sub elements rule integration

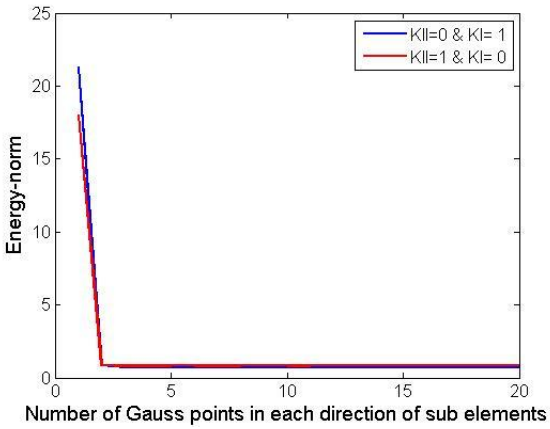

Figure 10(b). Convergence in the Energy norm for element type 1 by Sub elements rule integration

Elements type 2, 3 and 4

As declared in Figure 5, in these elements crack tip enrichment is executed in a number of nodes. In order to calculate errors related to stiffness matrix integration were executed by means of trapezoidal and Gauss Quadrature rules. Stiffness matrix errors are shown in Figures 11 and 12.

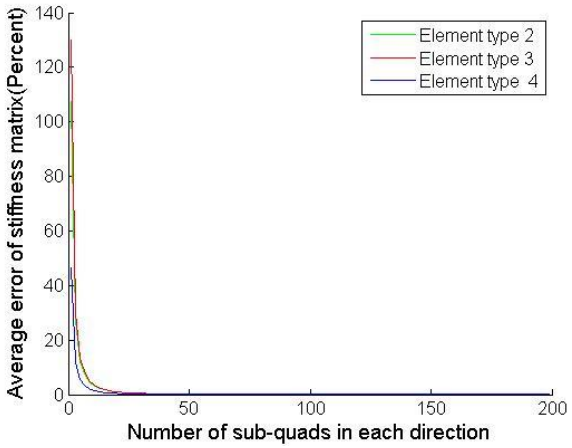

Figure 11(a). Average error of stiffness matrix by Trapezoidal rule integration, related to Element's type 2, 3 and 4

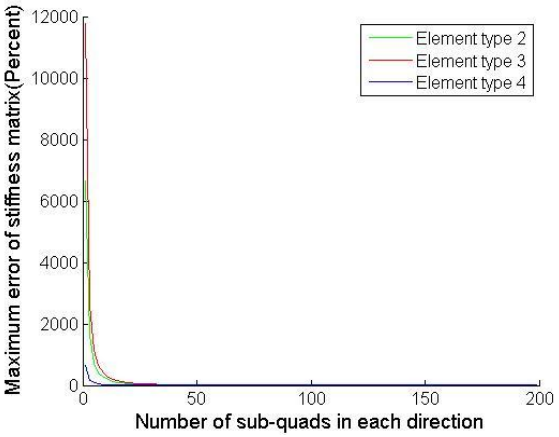

Figure 11(b). Maximum error of stiffness matrix by Trapezoidal rule integration, related to Element's type 2, 3 and 4

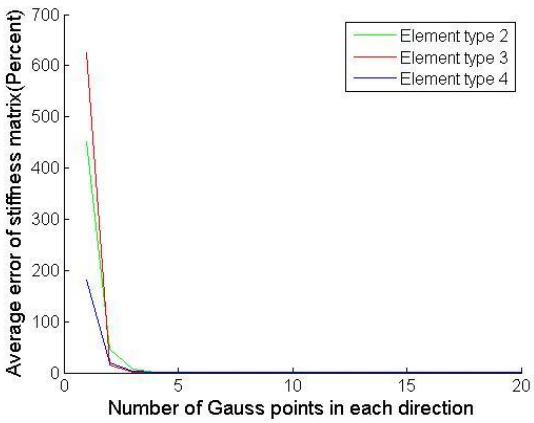

Figure 12(a). Average error of stiffness matrix by Gauss Quadrature integration, related to Element's type 2, 3 and 4

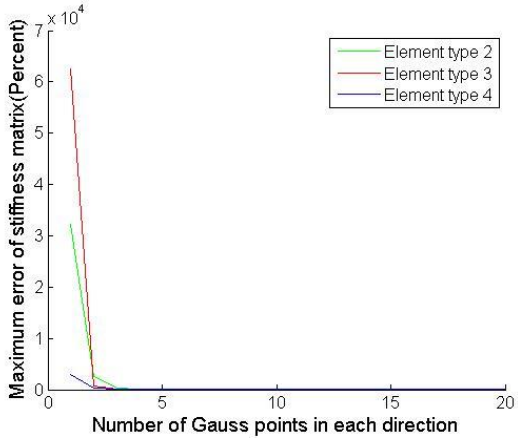

Figure 12(b). Maximum error of stiffness matrix by Gauss Quadrature integration, related to Element's type 2, 3 and 4

Tables 2, 3 and 4 show required number of sampling points using different integration rules leading to 1, 2, 5 and 10 percent errors for element types 2, 3 and 4, respectively.

Table 2. Required minimum sampling points number to achieve different errors in element type 2

Type of integration	Trapezo-idal rule	Gauss Quadra-ture rule
Required number of sampling points to achieve a less than 1% average error	20*20	5*5
Required number of sampling points to achieve a less than 1% maximum error	153*153	7*7
Required number of sampling points to achieve a less than 2% average error	14*14	4*4
Required number of sampling points to achieve a less than 2% maximum error	111*111	6*6
Required number of sampling points to achieve a less than 5% average error	9*9	4*4
Required number of sampling points to achieve a less than 5% maximum error	71*71	6*6
Required number of sampling points to achieve a less than 10% average error	6*6	3*3
Required number of sampling points to achieve a less than 10% maximum error	50*50	5*5

Table 3. Required minimum sampling points number to achieve a different error in element type 3

Type of integration	Trapezo-idal rule	Gauss Quadra-ture rule
Required number of sampling points to achieve a less than 1% average error	21*21	4*4
Required number of sampling points to achieve a less than 1% maximum error	185*185	5*5
Required number of sampling points to achieve a less than 2% average error	15*15	4*4
Required number of sampling points to achieve a less than 2% maximum error	136*136	5*5
Required number of sampling points to achieve a less than 5% average error	9*9	3*3
Required number of sampling points to achieve a less than 5% maximum error	87*87	5*5
Required number of sampling points to achieve a less than 10% average error	7*7	3*3
Required number of sampling points to achieve a less than 10% maximum error	62*62	4*4

Table 4. Required minimum number of sampling points to achieve different errors in element type 4

Type of integration	Trapezo-idal rule	Gauss Quadra-ture rule
Required number of sampling points to achieve a less than 1% average error	14*14	4*4
Required number of sampling points to achieve a less than 1% maximum error	53*53	6*6
Required number of sampling points to achieve a less than 2% average error	9*9	4*4
Required number of sampling points to achieve a less than 2% maximum error	37*37	5*5
Required number of sampling points to achieve a less than 5% average error	6*6	3*3
Required number of sampling points to achieve a less than 5% maximum error	23*23	5*5
Required number of sampling points to achieve a less than 10% average error	5*5	3*3
Required number of sampling points to achieve a less than 10% maximum error	16*16	5*5

Since average error in element type 2 is less than 1% using a 4*4 network integrated by Gauss Quadrature rule and also considering that maximum error in stiffness matrix is not very effective on calculations, one may say that in order to execute minimum such calculations using a 4*4 network integrated by Gauss Quadrature rule, a desired accuracy in calculating stiffness matrix of elements is achieved, while the crack tip enrichment is also executed.

It should be stated that in determining all error criteria, different element sizes were studied and we observed that element's size has no effect on error quantity.

Element type 5

As in Figure 5, this type of element is divided into two parts by the crack and the crack tip enrichment together with discontinuity enrichment are executed in the corresponding nodes. In order to calculate errors related to stiffness matrix the integration was done by trapezoidal, Gauss Quadrature and sub element rules.

When using sub element rule, as shown in Figure 13, the element was divided into 2 sub elements and integration was carried out in each sub element. A range of 2*2 to 20*20 networks were considered as sampling points in each sub element. Accordingly, the computed stiffness matrix errors are shown in Figures 14, 15 and 16.

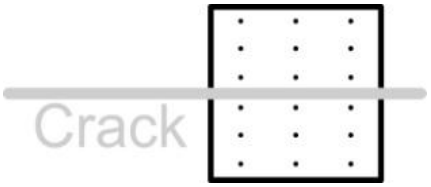

Figure 13. Sub elements of element type 5 and 7

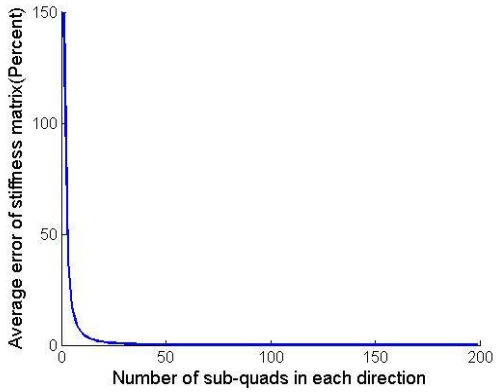

Figure 14(a). Average error of stiffness matrix by Trapezoidal rule integration, related to Element's type 5

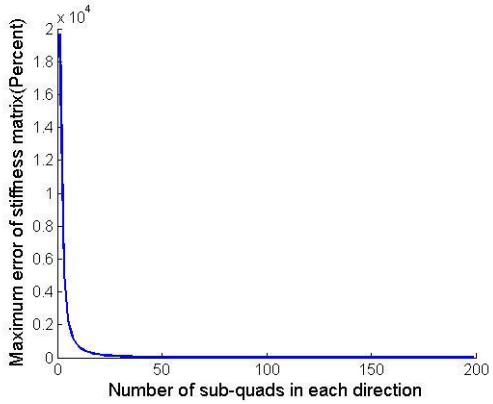

Figure 14(b). Maximum error of stiffness matrix by Trapezoidal rule integration, related to Element's type 5

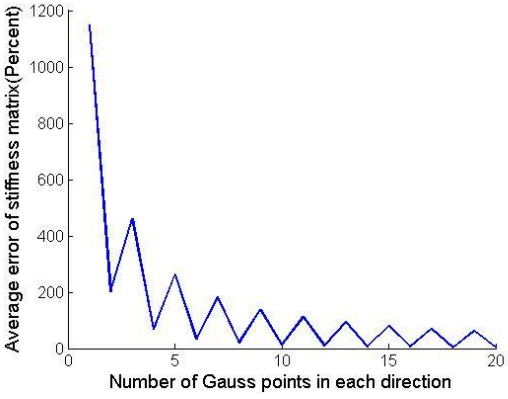

Figure 15(a). Average error of stiffness matrix by Gauss Quadrature integration, related to Element's type 5

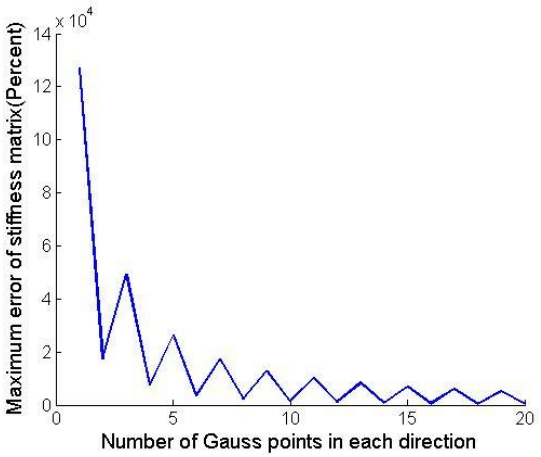

Figure 15(b). Maximum error of stiffness matrix by Gauss Quadrature integration, related to Element's type 5

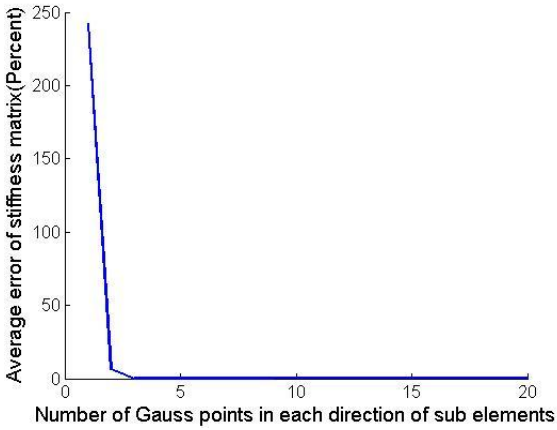

Figure 16(a). Average error of stiffness matrix by Sub elements rule integration, related to Element's type 5

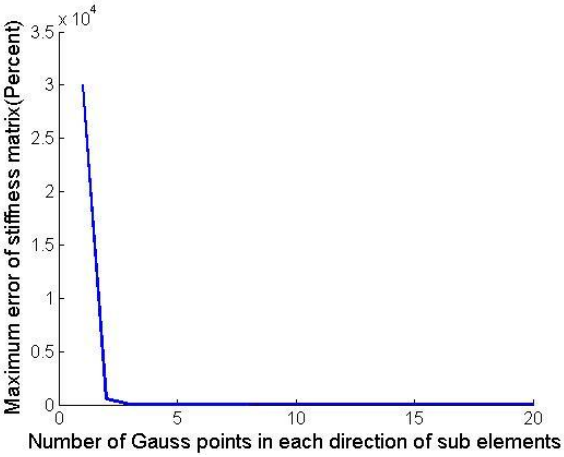

Figure 16(b). Maximum error of stiffness matrix by Sub elements rule integration, related to Element's type 5

As indicated earlier in Figure 7, element 1 resulted in a disturbance recounted to Gauss Quadrature rule. This is due to the fact that when odd number sampling points are selected, the mid points are placed on discontinuity boundary. Thus when solving numerically, significant errors appear.

In element type 5 if we use trapezoidal integration, considering a 25*25 network which means executing calculations for 625 points, average or even maximum errors do not reach 1% in stiffness matrix. But if we use Gauss Quadrature, average and maximum errors in stiffness matrix never reaches a less than 1%.

However, by using sub element rule, a less than 1% average and maximum errors are obtained with only a 3*3 and 5*5 networks, respectively. This means by carrying calculations for only 18 and 25 points, a less than 1% average and maximum errors in stiffness matrix will be performed, respectively.

Number of required sampling points to reach 2%, 5% and 10% errors were preceded and are listed in Table 5.

Table 5. Required minimum sampling points number to achieve different errors in element type 5

Type of integration	Trapezoidal rule	Gauss Quadrature rule	Sub elements rule
Required number of sampling points to achieve a less than 2% average error	17*17	---	2*5*5
Required number of sampling points to achieve a less than 2% maximum error	188*188	---	2*3*3
Required number of sampling points to achieve a less than 5% average error	11*11	18*18	2*4*4
Required number of sampling points to achieve a less than 5% maximum error	124*124	---	2*3*3
Required number of sampling points to achieve a less than 10% average error	7*7	12*12	2*4*4
Required number of sampling points to achieve a less than 10% maximum error	89*89	---	2*2*2

Element type 6

Figure 5 performs crack tip and discontinuity enrichments for the nodes of type 6 element. In order to investigate on the stiffness matrix's error, integration is executed by trapezoidal and Gauss Quadrature rule. Results of which are illustrated in Figures 17 and 18.

Number of required sampling points to reach 1%, 2%, 5% and 10% errors are shown in Table 6.

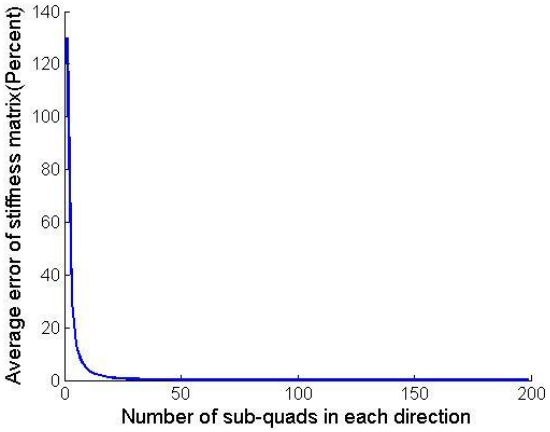

Figure 17(a). Average error of stiffness matrix by Trapezoidal rule integration, related to Element's type 6

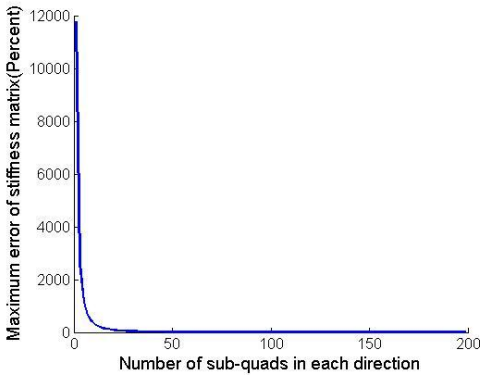

Figure 17(b). Maximum error of stiffness matrix by Trapezoidal rule integration, related to Element's type 6

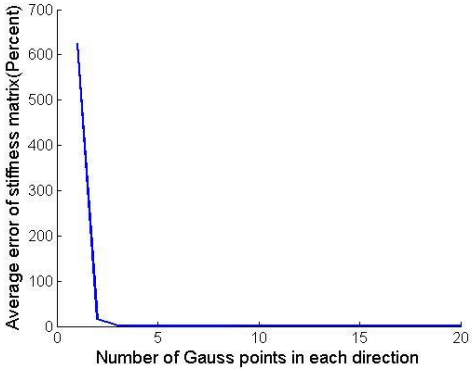

Figure 18(a). Average error of stiffness matrix by Gauss Quadrature integration, related to Element's type 6

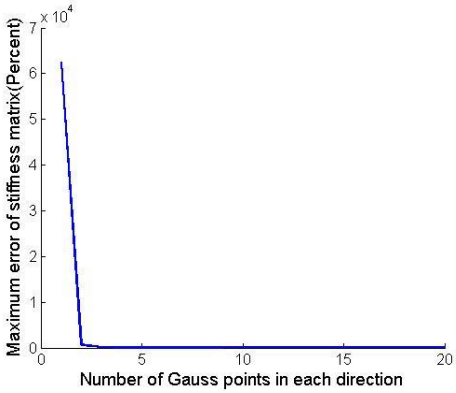

Figure 18(b). Maximum error of stiffness matrix by Gauss Quadrature integration, related to Element's type 6

Table 6. Required minimum sampling points number to achieve a different error in element type 6

Type of integration	Trapezoidal rule	Gauss Quadrature rule
Required number of sampling points to achieve a less than 1% average error	21*21	4*4
Required number of sampling points to achieve a less than 1% maximum error	185*185	5*5
Required number of sampling points to achieve a less than 2% average error	15*15	3*3
Required number of sampling points to achieve a less than 2% maximum error	136*136	5*5
Required number of sampling points to achieve a less than 5% average error	9*9	3*3
Required number of sampling points to achieve a less than 5% maximum error	88*88	5*5
Required number of sampling points to achieve a less than 10% average error	7*7	3*3
Required number of sampling points to achieve a less than 10% maximum error	62*62	4*4

Element type 7

This element's condition is similar to that of type 5 however, here only discontinuity enrichment is carried out. The error computation on the element's nodes was carried out using trapezoidal, Gauss Quadrature and sub element rules. Stiffness matrix's errors are shown in Figures 19, 20 and 21.

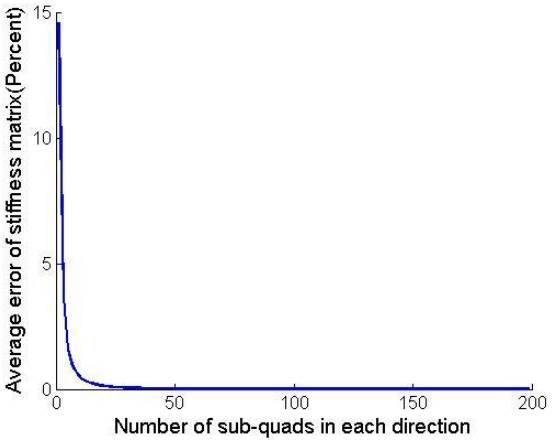

Figure 19(a). Average error of stiffness matrix by Trapezoidal rule integration, related to Element's type 7

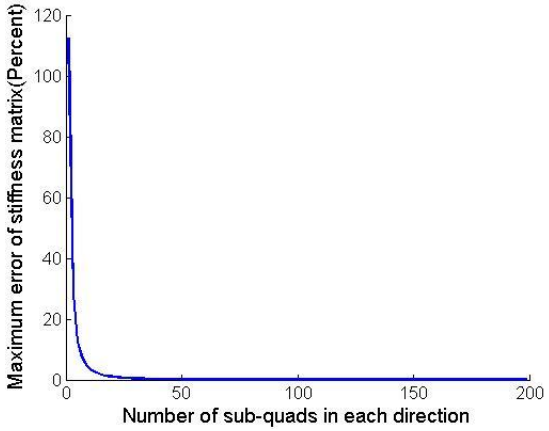

Figure 19(b). Maximum error of stiffness matrix by Trapezoidal rule integration, related to Element's type 7

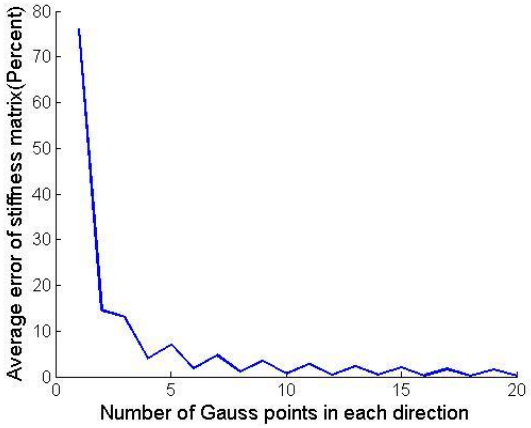

Figure 20(a). Average error of stiffness matrix by Gauss Quadrature integration, related to Element's type 7

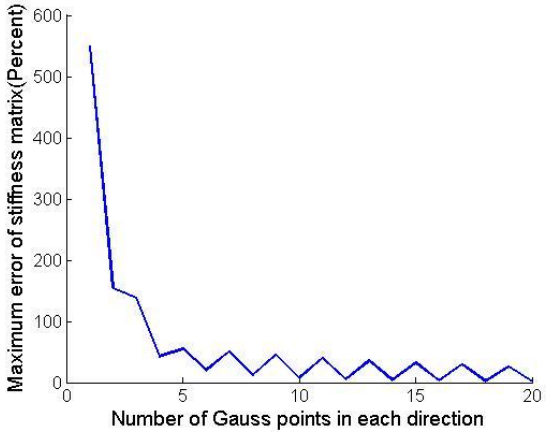

Figure 20(b). Maximum error of stiffness matrix by Gauss Quadrature integration, related to Element's type 7

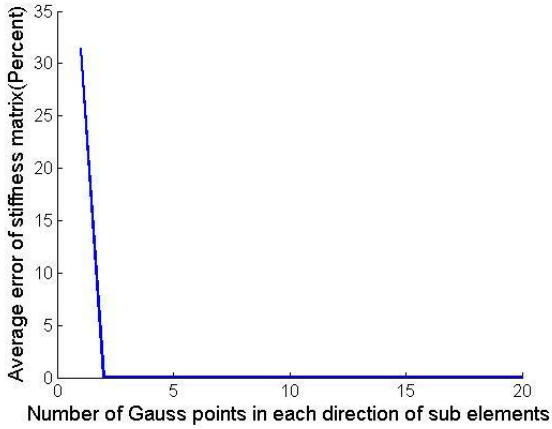

Figure 21(a). Average error of stiffness matrix by Sub elements rule integration, related to Element's type 7

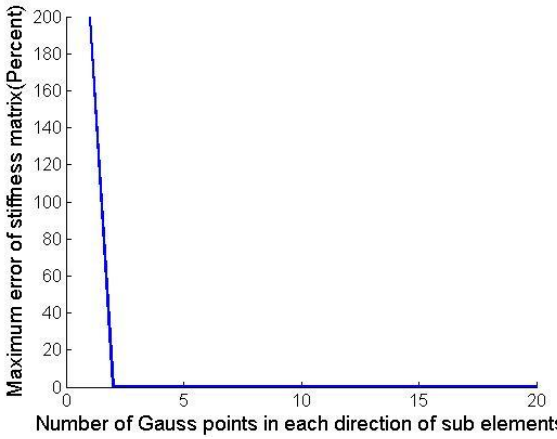

Figure 21(b). Maximum error of stiffness matrix by Sub elements rule integration, related to Element's type 7

In element type 7 if we use trapezoidal integration for a 7*7 and 21*21 networks, average and maximum errors in stiffness matrix would be found less than 1%. Using Gauss Quadrature integration, an average error of below 1% is achieved with even numbers of sampling points higher than 10*10 networks. Maximum error in stiffness matrix never lowers to a less than 1%. However, in case of using sub element rule with just a 2*2 network in each sub element which means executing calculations for only 8 points, stiffness matrix performs an exact solution.

Element type 8

For this type of the element only discontinuity enrichment is done. In order to calculate errors related to stiffness matrix, integration is done by trapezoidal and Gauss Quadrature rule. Stiffness matrix errors are shown in Figures 22 and 23.

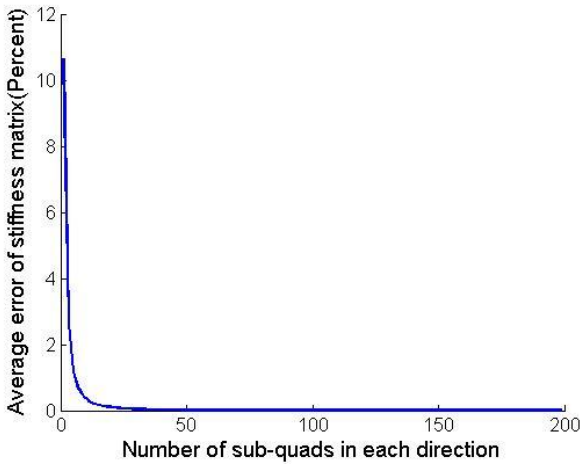

Figure 22(a). Average error of stiffness matrix by Trapezoidal rule integration, related to Element's type 8

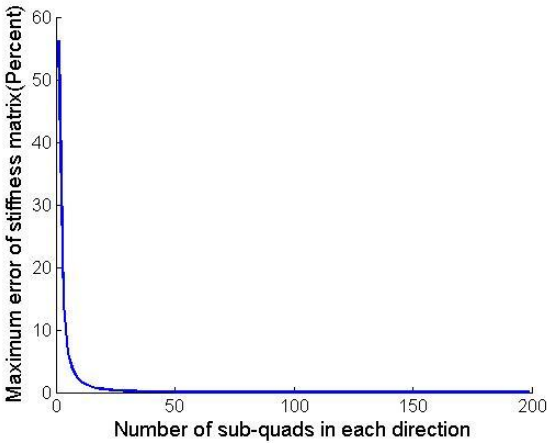

Figure 22(b). Maximum error of stiffness matrix by Trapezoidal rule integration, related to Element's type 8

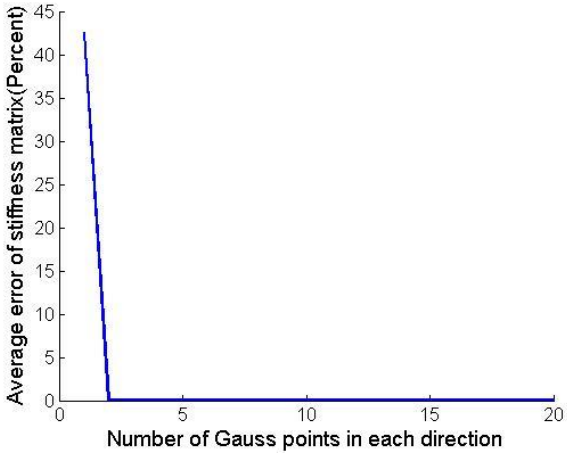

Figure 23(a). Average error of stiffness matrix by Gauss Quadrature integration, related to Element's type 8

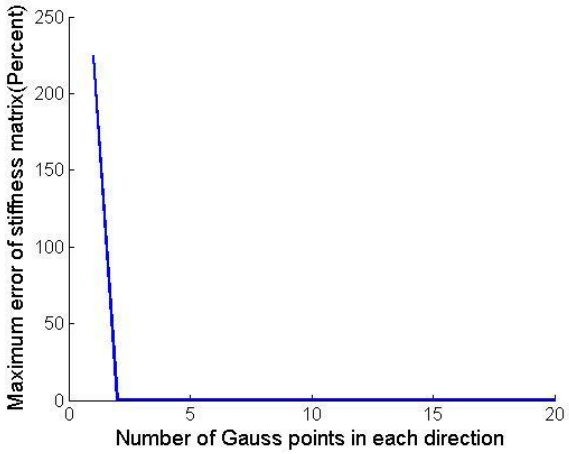

Figure 23(b). Maximum error of stiffness matrix by Gauss Quadrature integration, related to Element's type 8

For element type 8 if using a trapezoidal integration considering a 6*6 network, average error in stiffness matrix reaches a value less than 1% and by considering a 15*15 network, maximum error in stiffness matrix would be less than 1%. In case of using Gauss Quadrature, a 2*2 network in each element results an exact solution for the stiffness matrix.

Calculation of SIFs

Since in calculations related to cracked structures one of the most important goals is to calculate stress intensity factor (SIF) which is the criterion of crack's propagation, at this part we study the effect of integration error on created error at this coefficient.

Here, SIFs are computed using domain form of the interaction energy integral owing to the following advantages. This approach is based on the path independent J -integral (Rice, 1968) and thus, it is mesh independent (Dhondt, 2001). Further, it can be easily integrated into a finite element code, and does not require any mesh rearrangement near crack tip unlike some other methods, such as virtual crack extension (Delorenzi, 1985), or virtual crack closure integral (Buchholz et al., 1988).

The interaction integral is the sum of two cinematically admissible states of a cracked structure. State 1 $(\sigma_{ij}^{(1)},\varepsilon_{ij}^{(1)},u^{(1)},v^{(1)})$ corresponds to the actual state, whereas state 2 $(\sigma_{ij}^{(2)},\varepsilon_{ij}^{(2)},u^{(2)},v^{(2)})$ corresponds to an auxiliary state, which can be the asymptotic crack tip fields for either mode I or mode II from equations 9 and 11, respectively.

The domain form of interaction integral is shown in Figure 24 and is given by (Edke and Chang, 2011):

$$I^{(1,2)} = \int_A \left[\sigma_{xx}^{(1)} \frac{\partial u^{(2)}}{\partial x} \frac{\partial q}{\partial x} + \sigma_{xy}^{(1)} \frac{\partial u^{(2)}}{\partial x} \frac{\partial q}{\partial y} + \sigma_{xy}^{(1)} \frac{\partial v^{(2)}}{\partial x} \frac{\partial q}{\partial x} + \sigma_{yy}^{(1)} \frac{\partial v^{(2)}}{\partial x} \frac{\partial q}{\partial y} \right] dA + \int_A \left[\sigma_{xy}^{(2)} \frac{\partial u^{(1)}}{\partial x} \frac{\partial q}{\partial y} + \sigma_{xx}^{(2)} \frac{\partial v^{(1)}}{\partial x} \frac{\partial q}{\partial y} - \sigma_{xy}^{(2)} \frac{\partial u^{(1)}}{\partial y} \frac{\partial q}{\partial x} - \sigma_{yy}^{(2)} \frac{\partial v^{(1)}}{\partial y} \frac{\partial q}{\partial x} \right] dA \quad (12)$$

To cite this paper: H.Ghohani Arab, M.R. Ghasemi, 2013. Errors Estimation of Different Numerical Integration Techniques on Stiffness Matrix and Stress Intensity Factor in XFEM. *J. Civil Eng. Urban.*,*3* (5): 265-278.
Journal homepage: http://www.ojceu.ir/main/

where q is a weighting function, being equal to 1 on an open set containing the crack tip (Γ_1)and vanishes on the outer contour(Γ_2). The interaction energy integral is related to the SIFs as follows (Edke and Chang, 2011):

$$I^{(1,2)} = \frac{2}{E^*}\left(K_I^{(1)}K_I^{(2)} + K_{II}^{(1)}K_{II}^{(2)}\right) \quad (13)$$

where E^* assumes the value of $E/(1-\nu^2)$ and $E/2(1+\nu)$ for plane stress and plane strain states, respectively. To obtain mode I SIF, the auxiliary state (state 2) is chosen to be the pure mode I condition. Substituting $K_I^{(2)}=1$ and $K_{II}^{(2)}=0$ in the above equation gives:

$$K_I^{(1)} = \frac{E^*}{2} I^{(1.ModeI)} \quad (14)$$

where $I^{(1,\text{Mode I})}$, is the interaction integral for the actual state and mode I state. Field variables for the actual state ($\sigma_{ij}^{(1)},\varepsilon_{ij}^{(1)},u^{(1)},v^{(1)}$) are obtained by the XFEM solution and those for auxiliary mode I state are obtained by directly substituting $K_I^{(2)}=1$ and $K_{II}^{(2)}=0$ in equations 9 and 11. In a similar manner, mode II SIF can be obtained by directly substituting $K_I^{(2)}=0$ and $K_{II}^{(2)}=1$ in equations 9 and 11.

$$K_{II}^{(1)} = \frac{E^*}{2} I^{(1.Mode2)} \quad (15)$$

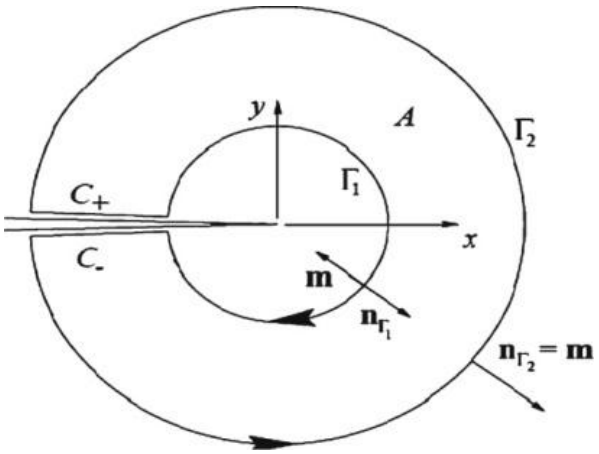

Figure 24. Interaction integral converted into domain form (Edke and Chang, 2011)

In this part an edge cracked plate in dimensions of 2*2 is considered similar to Figure 25. In order to do XFEM calculations this plate is meshed by a 19*19 network. Amounts of displacement of boundary nodes of this network is calculated by means of equation 9 for conditions ($K_I=1$ and $K_{II}=0$) and ($K_I=0$ and $K_{II}=1$). After executing XFEM calculations amounts of K_I and K_{II} is calculated by interaction integral method for each condition.

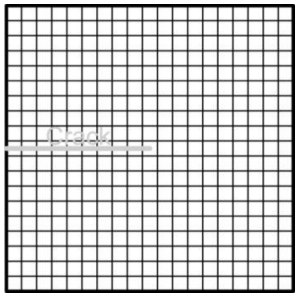

Figure 25. Structured mesh for edge cracked plate

In calculations related to stiffness matrix integration, considering related results of stiffness matrix errors, for integrations elements of type 2, 3, 4 and 6 is done by Gauss Quadrature considering a 5*5 network. In case elements type 5 and 7 sub elements rule is applied based on pattern shown in Figure 13 which we have used a 5*5 and 2*2 networks gradually in each sub element. Element 1 integration was done by sub element rule based on pattern shown in Figure 8. Relation between number of integration point's network in sub elements of element type 1 and calculated SIF is shown in Figure 26.

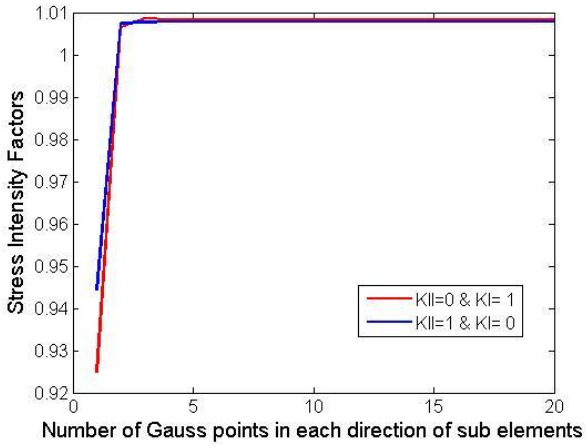

Figure 26. Convergence in stress intensity factors by Sub elements rule integration in element type 1

Considering this Figure it is clear that increase in integration points to more than 3*3 networks in each sub element is not effective on calculations' general result.

Amount of SIFs are studied by several meshes and results are shown in Table 7. In order to calculate stiffness matrix, for integration of elements type 2, 3, 4 and 6 we have used Gauss Quadrature rule considering a 5*5 network. In case elements type 5 and 7 we have used sub element rule based on patterns shown in Figure 13 which are gradually 5*5 and 2*2 for each sub element. For element type 8 we have used Gauss Quadrature rule considering a 2*2 network. Element 1's integration was done by means of sub element rule based on patters shown in Figure 8 which a 5*5 network was used for each sub element.

Table 7. Relation between element's size and calculated SIFs

Number of elements in mesh	$K_I/K_{I(exact)}$	$K_{II}/K_{II(exact)}$
5*5	0.5368	0.5428
9*9	1.0174	1.0143
15*15	1.0112	1.01
19*19	1.0091	1.0082
25*25	1.0071	1.0066
29*29	1.0063	1.0058
35*35	1.0053	1.0049

CONCLUSION

Nodal enrichment of different types of elements were studied using different integration rules in the analysis of cracked structure using eXtended Finite Element Method.

Regarding elements with only discontinuity enrichment on their corresponding nodes, Gauss Quadrature technique was applied by means of a 2*2 integration network as a result of which an exact solution was executed. This was due to the fact that the new shape functions remained linear after the enrichment.

In case of an element with only discontinuity enrichment applied to its corresponding nodes while the element was divided into two parts by a crack, sub element rule was applied and a 2*2 integration network was executed in each sub element. Results performed an exact solution. This could be due to the fact that the new shape functions remained linear after the enrichment.

In case of enhancing an element with discontinuity and singularity enrichments applied to its corresponding nodes, executing Gauss Quadrature technique on a 5*5 integration network, a mean error of less than 1% was obtained on the stiffness matrix. The reason for such an even though minor error could be due to the nonlinearity behavior of nodal shape functions after enrichments.

Concerning elements with singularity enrichment applied to their corresponding nodes while the elements were divided into two parts by a crack, or tip of crack is located inside one element, using sub element rule on a 5*5 integration network, applied to each sub element, a less than 1% mean error was detected on the stiffness matrix. The reason for the existence of this minor error could be due to the nonlinearity behavior of nodal shape functions after enrichments.

Studies also indicated that size of element does not affect the accuracy of stiffness matrix computation.

It is important to note that using Gauss Quadrature technique for the elements, being divided into two parts by the crack or the crack tip is placed inside them, an exact solution cannot be met. Therefore it is emphasized that if sub element rule is not used for these elements, trapezoidal integration rule may perform better results.

Also the present study performed the fact that even SIF calculation is not affected by the 1% error in stiffness matrix and the accuracy of results are manipulated by the element size.

REFERENCES

1. Fries, TP, Belytschko T. (2010). The extended/ generalized finite element method: An overview of the method and its applications. International Journal for Numerical Methods in Engineering, 84(3): 253-304.
2. Belytschko, T, Liu, WK, Moran, B. (2000). Nonlinear Finite Elements for Continua and Structures, John Wiley & Sons, Chichester.
3. Zienkiewicz, OC, Taylor, RL. (2000). The Finite Element Method, volume 1 – 3, Butterworth-Heinemann, Oxford.
4. Moës, N, Dolbow, J, Belytschko, T. (1999). A finite element method for crack growth without remeshing. International Journal for Numerical Methods in Engineering, 46: 131-150.
5. Mohammadi, S. (2008). Extended finite element method for fracture analysis of structures, Blackwell, Oxford.
6. Melenk, JM, Babuska, I. (1996). The Partition of Unity Finite Element Method: Basic Theory and Applications. Seminar fur Angewandte Mathematik, Zurich, Switzerland.
7. Duarte, CA, Oden, JT. (1996). An H-p adaptive method using clouds. Computer Methods in Applied Mechanics and Engineering, 139: 237-262.
8. Belytschko, T, Black, T. (1999). Elastic crack growth in finite elements with minimal remeshing. International Journal of Fracture Mechanics, 45(5): 601-620.
9. Dolbow, J. (1999). An extended finite element method with discontinuous enrichment for applied mechanics, PhD dissertation, Theoretical and Applied Mechanics, Northwestern University, USA.
10. Dolbow, J, Moës, N, Belytschko, T. (2000). Discontinuous enrichment in finite elements with a partition of unity method. Finite Elements in Analysis and Design, 36(3-4): 235-260.
11. Dolbow, J, Moës, N, Belytschko, T. (2000). Modeling fracture in Mindlin–Reissner plates with the extended finite element method. International Journal of Solids and Structures, 37(48): 7161-7183.
12. Dolbow, J, Moës, N, Belytschko, T. (2001). An extended finite element method for modeling crack growth with frictional contact. Computer Methods in Applied Mechanics and Engineering, 190(51-52): 6825-6846.
13. Daux, C, Moës, N, Dolbow, J, Sukumark, N, Belytschko, T. (2000). Arbitrary branched and intersecting cracks with the extended finite element method. International Journal for Numerical Methods in Engineering, 48(12): 1741–1760.
14. Sukumar, N, Moës, N, Moran, B, Belytschko, T. (2000). Extended finite element method for three-dimensional crack modeling. International Journal for Numerical Methods in Engineering, 48(11): 1549–1570.
15. Motamedi, D, Mohammadi, S. (2010). Dynamic analysis of fixed cracks in composites by the extended finite element method. Engineering Fracture Mechanics, 77(17): 3373-3393.
16. Pommier, S, Gravouli, A, Combescure, A, Moës, N. (2011). Extended finite element method for crack propagation, Wiley, Hoboken.
17. Dolbow, J, Nadeau, JC. (2002). On the use of effective properties for the fracture analysis of microstructured materials. Engineering fracture mechanics, 69(14-16): 1607-1634.
18. Bayesteh, H, Mohammadi, S. (2013). XFEM fracture analysis of orthotropic functionally graded materials. Composites: Part B , 44: 8-25.
19. Sukumar, N, Prévost, JH. (2003). Modeling quasi-static crack growth with the extended finite element method Part I: Computer implementation. International Journal of Solids and Structures, 40: 7513–7537.
20. Asadpoure, A, Mohammadi, S, Vafai, A. (2006). Modeling crack in orthotropic media using a coupled finite element and partition of unity methods. Finite Elements in Analysis and Design, 24(13): 1165 - 1175.
21. Laborde, P, Pommier, J, Renard, Y, Salaün, M. (2005). High-order extended finite element method

for cracked domains. International Journal for Numerical Methods in Engineering, 64(3): 354-381.
22. Béchet, E, Minnebo, H, Moës, N, Burgardt, B. (2005). Improved implementation and robustness study of the X-FEM for stress analysis around cracks. International Journal for Numerical Methods in Engineering, 64(8): 1033-1056.
23. Fries, TP, Belytschko, T. (2007). The intrinsic partition of unity method. Computational Mechanics, 40(4): 803-814.
24. Anderson, TL. (1985). Fracture mechanics: fundamentals and applications, CRC, Boca Raton.
25. Rice, JR. (1968). A path independent integral and the approximate analysis of strain concentration by notches and cracks. Journal of Applied Mechanics, 35(2): 379-386.
26. Dhondt, G. (2001). 3-D mixed-mode K-calculations with the interaction integral method and the quarter point element stress method. Communications in Numerical Methods in Engineering, 17(5): 303–307.
27. deLorenzi, HG. (1985). Energy release rate calculations by the finite element method. Engineering Fracture Mechanics, 21: 129-143.
28. Buchholz, FG, Grebner, H, Dreyer, KH, Krome, H. (1988). 2D and 3D applications of the improved and generalized modified crack closure integral method. Computational Mechanics, 1: 1-14.
29. Edke, MS, Chang, KH. (2011). Shape optimization for 2-D mixed-mode fracture using Extended FEM (XFEM) and Level Set Method (LSM). Structural and Multidisciplinary Optimization, 44(2): 165-181.